Soft Matter

PAPER

View Article Online
View Journal | View Issue

Cite this: Soft Matter, 2016, 12, 9377

Cylindrical chains of water drops condensing on microstructured lubricant-infused surfaces†

Tadashi Kajiya,‡[a] Sanghyuk Wooh,‡[a] Yunchan Lee,[b] Kookheon Char,[b] Doris Vollmer[a] and Hans-Jürgen Butt*[a]

Received 15th August 2016,
Accepted 30th October 2016

DOI: 10.1039/c6sm01883a

www.rsc.org/softmatter

We studied the condensation of water drops on a micro-structured lubricant-infused surfaces. Hierarchical micro-prism surfaces were fabricated by soft imprinting with wet TiO_2 nanoparticle paste. After hydrophobization, the patterned surfaces were infused with silicone oil as a lubricant. When cooling at high humidity (over 80%), water drops nucleate and start growing on the surface. Once they have reached a certain size, the drops at neighboring channels of the micro-prisms attract each other and spontaneously form cylindrical chains. These chains of drops align perpendicular to the prism array. The morphology and the length-to-width ratio of the chains of drops depend on the thickness of the lubricant layer. This new concept of water drop alignment on lubricant-infused surfaces offers a new route for pattern formation with condensed drops.

I. Introduction

Condensation of water drops from the atmosphere onto a solid surface is a daily-observed phenomenon. Dew in the morning and fogging of glasses and windscreens are typical examples. Condensation has been generally studied in technological applications for thermal management and heat transfer in power generation[1] and continuous water harvesting by dew or fog.[2–4]

Condensed drops are also used to pattern surfaces known as breath figures[5,6] and to fabricate micro-particles[7]. When blowing humid air over a polymer solution whose solvent has a low boiling point and is immiscible with water, evaporative cooling leads to the condensation of water drops at the surface of the polymer solution. These drops can form a hexagonal array. After evaporation of the liquids, a hexagonal array of bubbles is left in the polymer. In this way, regular arrays of pores in a polymer film can be prepared.[8,9]

Research on the condensation has been extended to lubricant-infused surfaces. These micro- or nano-textured surfaces are infused with a non-volatile lubricant of low surface tension.[10–12] A thin lubricant layer covers the solid substrate and is kept in place by capillary forces. When placing a drop of an immiscible liquid on a lubricant-infused surface, the drops slide off at tilt angles of a few degrees.[13–15] Anaud *et al.* and Park *et al.* have shown the facile collection of condensed drops.[16,17] Kim *et al.* demonstrated the good anti-icing properties,[18] as the drops are removed before ice-formation sets in.

In our previous work, we imaged the condensation of water drops onto lubricant-infused square arrays of micro-pillars by confocal microscopy.[19] Here, we describe the condensation dynamics of water drops on lubricant-infused porous surfaces with a hierarchical nano- and microstructure. Rather than the 2D regular arrays, we used a 1D symmetry. The surface consists of linear arrays of TiO_2 micro-prisms with nanometer-sized porosity, which is infused with silicone oil. While condensing, the water drops aligned perpendicular to the prism arrays and form long cylindrical chains. Micro-structuring the lubricant infused surface leads to the self-assembly of condensing drop. We investigate how the shape of chains depends on the parameters such as the thickness of the lubricant. We also discuss the mechanisms of chain droplet formation.

II. Materials and methods

The micro-prism patterned mesoporous titanium dioxide (TiO_2) surfaces (Fig. 1a) were prepared by soft-lithography using wet TiO_2 nanoparticle paste, following the procedure described by Kim *et al.*[20] and Wooh *et al.*[21,22] TiO_2 nanoparticle paste (18NR-T, Dyesol, particle diameter: 20 nm) was blade coated on a silicon wafer and then gently imprinted with a micro-prism patterned polydimethylsiloxane (PDMS) mold. The PDMS mold consisted of micro-prism pattern with a peak-to-peak distance of 25 μm and a slope of 45°. The imprinted paste was annealed at 70 °C

[a] Max Planck Institute for Polymer Research, Ackermannweg 10, 55128 Mainz, Germany. E-mail: butt@mpip-mainz.mpg.de
[b] The National Creative Research Initiative Center for Intelligent Hybrids & the WCU Program of Chemical Convergence for Energy and Environment, School of Chemical and Biological Engineering, Seoul National University, Seoul 08826, Korea

† Electronic supplementary information (ESI) available. See DOI: 10.1039/c6sm01883a
‡ These authors contributed equally to this work.

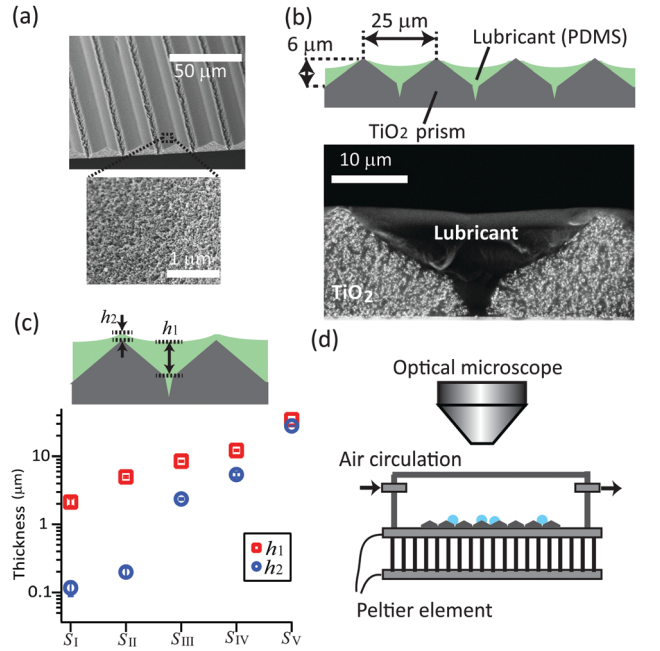

Fig. 1 (a) Scanning electron microscope (SEM) images of the micro-prism patterned mesoporous TiO_2 surface. The surface consists of a regular array of 2D prism patterns (top) that is mesoporous with ~10 nm size pores (bottom). (b) Schematic and SEM image of TiO_2 surface infused with silicone oil as lubricant. The silicone oil was spin-coated at 5000 rpm for 30 s. (c) Plot of the thickness of lubricant layer. The largest and smallest thickness (h_1, h_2) are plotted. The sample surfaces are, S_I: diluted silicone oil (by THF at 25 wt%) spin-coated at 5000 rpm. S_{II}: silicone oil spin-coated at 5000 rpm. S_{III}: spin-coated at 3500 rpm. S_{IV}: spin-coated at 2000 rpm. S_V: blade coated with 50 μm spacers. The SEM images of surfaces S_I (with thinnest lubricant layer) and S_V (with thickest lubricant layer) are shown as Fig. S1 (ESI†). (d) Setup for the water drop condensation.

for 10 min to evaporate solvent and to solidify the paste. After detaching the PDMS mold, the patterned TiO_2 paste was sintered at 500 °C for 30 min to decompose residual organics. The surface nano-roughness is necessary to keep the lubricant layer on the surface and provide a reservoir of lubricant. The surface was hydrophobized before coating with lubricant in order to prohibit the water drop adhering on the surface. For hydrophobization of the patterned surface, the surface was modified with trichloro(1*H*,1*H*,2*H*,2*H*-perfluorooctyl)silane by chemical vapor deposition for 2 hours in a pre-evacuated desiccator.

TiO_2 micro-prism arrays were infused with silicone oil (molecular weight: 9.7 kDa) by spin-coating for 30 s. The lubricant thickness was controlled by changing the rotation speed (2000, 3500 and 5000 rpm), or by diluting the silicone oil (25 wt%) with tetrahydrofuran (THF). In order to reach a lubricant thicknesses over 35 μm, silicone oil was applied by blade coating with 50 μm spacers.

The thickness of lubricant layers was measured using a cross-sectional scanning electron microscope (SEM, low voltage 1530 Gemini LEO, Zeiss) (Fig. 1b), after crosslinking the silicone oil on the surfaces. To crosslink, vinyl-terminated silicone oil with similar molecular weight (molecular weight: 9.4 kDa, viscosity: 0.2 Pass, DMS-V22 from Gelest Inc.) with a crosslinker (2 wt%, HMS-301 from Gelest Inc.) and a platinum catalyst (0.0125 wt%, SIP6831.2 from Gelest Inc.) was used. This crosslinkable silicone oil mixture was coated on the prism-patterned mesoporous surface and cut after 6 hours of curing at 60 °C. The volume shrinkage after crosslinking was below 1%. The silicone oil infiltrated the porous TiO_2 and also covered the micro patterns (Fig. 1b bottom). The thickness of the silicone oil layer at the bottom (h_1) and at the top (h_2) of prisms are plotted in Fig. 1c. While for sample S_I to S_{IV} the thickness varies and h_1 is lower than h_2, for sample S_V the micropattern is fully masked by the lubricant and $h_1 \approx h_2$.

The surface tensions of water (saturated with silicone oil) of $\gamma_w = 44$ mN m^{-1} and silicone oil (saturated with water) $\gamma_o = 20$ mN m^{-1} were measured using the pendant drop method (OCA35; DataPhysics, Germany).

Condensation of water drops was monitored using a video microscope (Nikon stereomicroscope SMZ-U with a 2× objective) connected to a CCD camera (Basler, model) (Fig. 1c). The temperature of the substrate was controlled with a Peltier module situated underneath the substrate. The sample was placed in a closed plastic chamber, under which a constant air flow at controlled humidity was circulated. To create an air flow with constant humidity (83 ± 3% at a temperature of 21 ± 1), a stream of dry and humid air (made by bubbling through a bottle filled with water) were mixed at controlled flow rates (20 ± 10 ml min^{-1} and 220 ± 15 ml min^{-1}). The substrate temperature was cooled down to 1 °C at a cooling rate of 0.25 ± 0.03 °C s^{-1}.

III. Results

Several stages of the condensation process could be distinguished (Fig. 2, supplemental Movie S1, ESI†):

– Nucleation and growth: after cooling was started, tiny water drops (dark elliptical spots) nucleate at random positions on the surface and grow (Fig. 2a). The light is coming from the left top side and illuminates the left flanks of the prisms (white areas). The dark areas correspond to the right flanks of the prisms (schematic (i)). Due to the surface geometry underneath the lubricant, water drops initially condense along the valleys of the prisms and grow individually.

– Attraction and formation of cylindrical chains of drops (Fig. 2b): drops that nucleated in the same valley of the prism come close and coalesce into bigger drops (schematic (ii) left). At the same time, drops in neighboring valleys attract and align at the same *y*-position. However, they do not coalesce (schematic (ii) right). The drops assemble into long cylindrical chains. In a chain, neighboring drops are separated by lamellae of silicone oil (Fig. 2c).

– Coalescence perpendicular to the prism: once the drops exceed a certain size, the drops within the cylindrically-shaped chains coalesce (schematic (iii)). These larger drops move in *x* direction and merge with neighboring drops one by one (Fig. 2d and e). When the coalesced drops have reached a radius of 3–5 times the prism spacing (Fig. 2d and e) they get pinned.

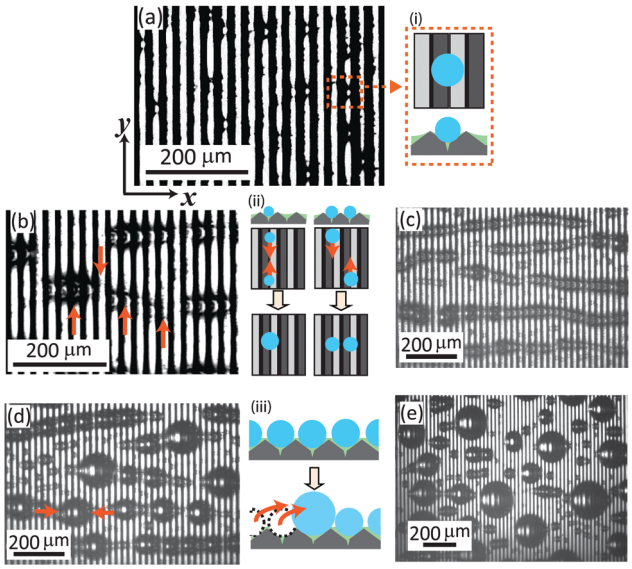

Fig. 2 Sequential optical microscope images of the condensing water drops on a prism-patterned lubricant infused surface (surface S_{III}). Images were acquired after (a) 40 s, (b) 80 s, (c) 120 s and (d) 360 s (e) 1000 s. The x axis is directed perpendicular to the prism lines and the y axis is parallel to the prism. (a) Initially, the drops nucleate randomly on the surface. As the light illuminates from the left top side, the white and black areas corresponds to the left and right flanks of the prisms, respectively (schematic (i)) (b) when the drops grow to a certain size, they interact attractively. Drops nucleated on the same prism line come close and merge (schematic (ii) left). The drops nucleated at the neighboring channels also attract, but they do not coalesce. As a result, they align to the same position on y axis (schematic (ii) right). (c) Finally, the drops form cylindrical chains. (d) and (e) At a last stage, coalescence occurs over the neighboring channel (schematic (iii)). Chains of drops merge to a large spherical drop.

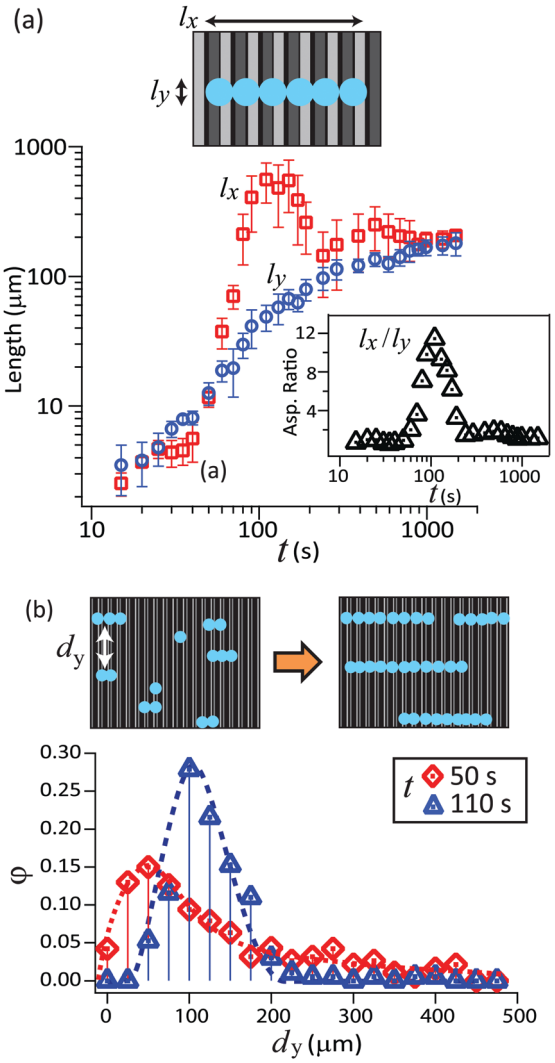

Fig. 3 (a) Plot of the two mean extension of the condensed drops. As illustrated in the schematic, l_x is perpendicular and l_y is parallel to the direction of the prisms (with surface S_{III}, $\bar{h}$ = 4.5 μm). The aspect ratio (l_x/l_y) is also plotted in the inset. (b) Probability distribution of the spacing between drops in y direction (d_y), obtained from multiple data on the surfaces S_{II} and S_{III}. Initially, the drops are distributed randomly in y direction (left schematic). With the formation of long cylindrical chains of drops, the spacing d_y becomes uniform, which is nearly 4 times bigger than the prism gap (right schematic).

Then, they only slide at tilt angles above 45°. Coalescence also creates new free surface and fresh nucleation occurs.

The length of the chains of drops l_x and width l_y are plotted as a function of time (Fig. 3a). l_x and l_y denote the maximum value measured in the x and y directions for each chain of drops.

At the early stage when the water drops nucleate and grow individually, the drops have a spherical cap shape. Therefore, the lengths l_x and l_y increase proportional to each other. The drops start attracting each other when the drop's diameter approaches roughly 5 μm, which is the order of prisms' height. Drops at neighboring prism channels align at the same y position, forming chains. Meanwhile, the individual drops in a chain grow together. It is not clear yet if the drops in a chain grow independently and just have a similar condensation kinetics, or if they are linked by diffusion of water from one drop to a neighboring one. l_x increases much faster than l_y at this stage, and the aspect ratio l_x/l_y exceeds 10. Finally, the chains of drops start to coalesce perpendicular to the prism. The chain-shaped drop transforms into a large spherical cap, therefore the aspect ratio l_x/l_y approaches unity.

We also analyzed how the drop–drop spacing changes with the creation of cylindrical-shaped chains of drops. For an ensemble of drops, we measured the distance of drops across the y axis (d_y). The value d_y is measured for adjacent cylindrical chains of drops which have an overlap at the same micro-prism channel. The probability distribution of d_y is plotted in Fig. 3b.

At the early stage ($t \leq 50$ s) just after the drop starts forming a chain of two or three drops, these drops are separated across the y axis at random. Measured spacing d_y is distributed in a broad range. As the alignment of drops continues (t = 50 s), the chains of drops are placed rather uniformly in y direction. The d_y distribution shows a sharp peak at $d_y = 100 \pm 5$ μm, which is 4 times larger than the pillar gap. To check how the geometry of the prism influences the formation of the cylindrical chains of drops, we condensed drops on lubricant-infused prism arrays with different peak-to-peak distances: 10 μm and 50 μm (Fig. S3, ESI†). The condensed drops form cylindrical chains on

all prism sizes. It turned out that the mean spacing d_y depends on the peak-to-peak distance of the micro-prism. d_y was roughly 4 times larger than the peak-to-peak distance.

IV. Discussion

We suggest that the self-assembly of drops to cylindrical chains originates from the competition between two mechanisms: capillary attraction and topological confinement (Fig. 4a). The high mobility of drops provided by the lubricant is a prerequisite.

On lubricant-infused surfaces, a water drops first nucleate on the free surface of lubricant.[19] In the early stage they form a liquid lens. Since the drops are small, one can neglect gravity and the two surfaces are shaped like spherical caps with two radii of curvature. These radii of curvature are given by $\gamma_w/R_w = \gamma_{lw}/R_{lw}$.[19,23] Here, γ_w is the surface tension of water saturated with silicon oil, γ_{lw} is the interfacial tension of the silicone oil/water interface, R_w is the radius of curvature of the top side of the lens and R_{lw} is the radius of curvature of the bottom side of the lens. After some time the lens has grown into a size that its bottom comes into contact with the TiO_2 surface. A solid three-phase contact line forms where the lubricant, TiO_2, and water meet. The creation of the solid contact line is indicated by the observation that the water drops do not slide down even when tilting the surface up to 45°.

After the water lens comes into contact with the hydrophobized TiO_2, further growth leads to an increase in circumference and in height. The fluid three-phase contact line, where water, lubricant and air meet, is shifted upward. The balance of the interfacial tensions creates the lubricant meniscus, found around the drop's perimeter, which has a negative curvature.[24] For isolated drops, the horizontal components of the surface tension of the lubricant/air interface cancel each other when integrating around the fluid contact line.[25] The surface tension dragging to the right is equal to the surface tension dragging to the left (Fig. 4a top). When a neighboring drop has grown large enough that the menisci start overlapping, the angle of the interface facing the second drop changes. It changes in such a way that the horizontal component increases (Fig. 4a middle). This leads to a net attractive force. Such phenomenon is similar to the lateral attraction between two particles which are suspended on a free liquid surface.[26–28]

Suppose that the lubricant fills the spacing between the micro-prisms up to slightly below the peaks of the prisms (surfaces S_{II} and S_{III}, Fig. 1). When the condensed water drops are smaller than the prism spacing, they are confined between the peaks of prisms. These drops are mobile along the valley of prisms (y direction), but the prism's peak hinders the drops to move perpendicularly (x direction). Meanwhile, the lubricant meniscus reaches the adjacent prism channel. Therefore, the drops in the neighboring channels start attracting each other. As a result, the drops are aligned in the x direction.

For a qualitative evaluation of the velocity, we consider the situation where the two cylindrical chains of length (l_I, l_{II}) and of width l_y approach each other at relative velocity v_y (Fig. 4b). Capillary attraction should occur only when the two menisci overlap. We denote the length where two chains overlap along the x axis as l_{ov}. The net attractive capillary force is mainly applied at this overlap region. The capillarity attractive force F_c is approximately given as,

$$F_c \approx l_{ov}\gamma_{lub}|\cos\theta_L - \cos\theta_R|. \quad (1)$$

Here, the angles θ_L and θ_R refer to the left and right slopes of the lubricant meniscus at the liquid contact line (Fig. 4a) with the drop and γ_{lub} is the surface tension of the lubricant. Following this attraction, the drops move towards each other. The speed is a balance between attraction and viscous friction. Assuming that viscous friction F_v is proportional to the chains lengths,

$$F_v \approx (l_I + l_{II})\frac{l_y}{d}v_y\eta, \quad (2)$$

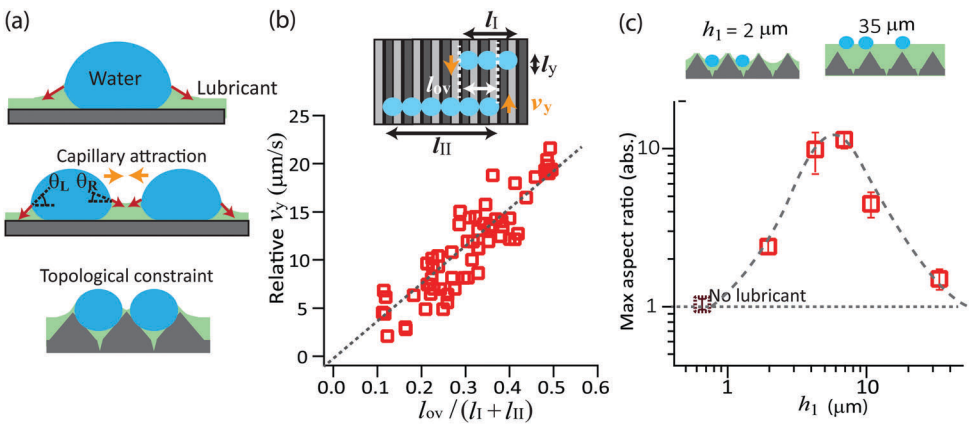

Fig. 4 (a) Mechanisms for the line drop formation; capillary attraction by the lubricant meniscus and topological confinement by the prism structure. (b) Relative y velocity (v_y) of two cylindrical chains of drops approaching each other. The data are plotted against the ratio of two lengths in x direction; the overlap length (l_{ov}) at which the two chains of drops overlap along x axis, and the total length ($l_I + l_{II}$). (c) Plot of the maximum value of the aspect ratio (l_x/l_y) *versus* the largest lubricant thickness (h_1). To achieve long cylindrical chains, there is an optimal lubricant thickness at 5 ± 2 μm, which is close to the prism height.

where η is the viscosity of the lubricant and d is the thickness of the lubricant layer beneath the drop. We obtain the relation,

$$\nu_y \approx \frac{l_{ov}}{l_I + l_{II}} \cdot \frac{\gamma_{lub}}{\eta}\left[\frac{|\cos\theta_L - \cos\theta_R|d}{l_y}\right]. \quad (3)$$

From multiple measurements on the surfaces S_{II} and S_{III}, we measured the relative velocity (ν_y) of two chains of drops which are attracting, and plotted as a function of the length ratio $l_{ov}/(l_I + l_{II})$. The proportionality was indeed observed (Fig. 4b). The prefactor $\gamma_{lub}d|\cos\theta_L - \cos_R|/(\eta l_y)$ in the example shown in Fig. 4b was 62 μm s^{-1}. With γ_{lub} = 0.02 N m^{-1}, η = 0.2 Pa s and $l_y \approx 50$ μm (twice the spacing of the microstructure) we estimate $d|\cos\theta_L - \cos_R| \approx 3$ nm. The angles of the meniscus at both sides of the chains are not largely different and we estimate that $|\cos\theta_L - \cos\theta_R|$ is of order 0.01 to 0.1. This leads to an estimate for the thickness of the lubricant layer beneath the drop of order 300 to 30 nm, neglecting contributions of the disjoining and Laplace pressure.

The formation of the cylindrical chains of drops is influenced by the thickness of the lubricant (Fig. 4c). If the lubricant thickness is very thin compared to the prism height, the lubricant meniscus does not reach the adjacent prism line. The onset of the attractive movement is delayed. Before the drops attract, they already grow sufficiently large to coalesce over the prism across the x axis. On the other hand, if the lubricant layer is thicker than the prism structure, the whole surface is completely covered. The condensed drops with their respective lubricant menisci are not anymore influenced by the topological confinement set by the prisms. The drops move in all directions, even perpendicular to the prism pattern. Once the drops come close, they simply merge into a large spherical cap drop.

Experimentally, we measured the maximum aspect ratio l_x/l_y on surfaces with different lubricant thickness, and plotted the maximum ratio as a function of the largest lubricant thickness h_1 (Fig. 4c). In order to achieve long chains of drops, we found that there is an optimal thickness of 7–9 μm, which corresponds to the depth of prism channels.

V. Conclusion

Water condensing on lubricant-infused surfaces patterned with linear micro-prisms forms parallel chains of drops. This hierarchical and spontaneous structural formation of water drops is caused by the lubricant film which provides a high mobility of the drops and a long-range capillary attraction. The water drops at the neighboring valleys of micro-prisms attract each other and align perpendicular to the prism array. With optimal lubricant thickness, long cylindrical-shaped chains of drops are formed, which are dispersed quite uniformly across the line. We suggest that such self-assembly of water drops originates from the capillary attraction by the lubricant meniscus and topological confinement set by the prisms. Our results imply that the use of lubricant-infused surfaces with specific surface geometry enables to realize patterns with condensing drops.

Acknowledgements

This project was funded by ERC for the advanced grant 340391-SUPRO. DV acknowledges support by COST1106. TK and SW acknowledges support by the Alexander Humboldt Foundation for financial support. TK greatly thanks Masao Doi and François Lequeux for theoretical discussion. KC acknowledges the financial supports from the National Research Foundation of Korea (NRF) for the National Creative Research Initiative Center for Intelligent Hybrids (no. 2010-0018290), the IRTG Program (no. 2011-0032203), and the World Class University Program of Chemical Convergence for Energy & Environment (R31-10013).

References

1 N. Miljkovic and E. N. Wang, *MRS Bull.*, 2013, **38**, 397–406.
2 K. S. Udell, *Int. J. Heat Mass Transfer*, 1985, **28**, 485–495.
3 A. R. Parker and C. R. Lawrence, *Nature*, 2001, **414**, 33–34.
4 D. Beysens, *C. R. Phys.*, 2006, **7**, 1082–1100.
5 C. Huang, T. Kamra, S. Chandhary and X. Shen, *ACS Appl. Mater. Interfaces*, 2014, **6**, 5971–5976.
6 A. Zhang, H. Bai and L. Li, *Chem. Rev.*, 2015, **115**, 9801–9868.
7 X. Xiong, W. Zou, Z. Yu, J. Duan, X. Liu, S. Fan and H. Zhou, *Macromolecules*, 2009, **42**, 9351–9356.
8 U. H. F. Bunz, *Adv. Mater.*, 2006, **18**, 973–989.
9 H. Bai, C. Du, A. Zhang and L. Li, *Angew. Chem., Int. Ed.*, 2013, **52**, 12240–12255.
10 A. Lafuma and D. Quéré, *Europhys. Lett.*, 2011, **96**, 56001.
11 T. S. Wong, S. H. Kang, S. K. Y. Tang, E. J. Smythe, B. D. Hatton, A. Grinthal and J. Aizenberg, *Nature*, 2011, **477**, 443–447.
12 J. D. Smith, R. Dhiman, S. Anand, E. Garduno, R. E. Cohen, G. H. McKinley and K. K. Varanasi, *Soft Matter*, 2013, **9**, 1772–1780.
13 F. Schellenberger, J. Xie, N. Encinas, A. Hardy, M. Klapper, P. Papadopoulos, H.-J. Butt and D. Vollmer, *Soft Matter*, 2015, **11**, 7617–7626.
14 X. Dai, B. B. Stogin, S. Yang and T.-S. Wong, *ACS Nano*, 2015, **9**, 9260–9267.
15 E. Jenner and B. D'Urso, *Appl. Phys. Lett.*, 2013, **103**, 251606.
16 S. Anand, A. T. Paxson, R. Dhiman, J. D. Smith and K. K. Varanasi, *ACS Nano*, 2012, **6**, 10122–10129.
17 K.-C. Park, P. Kim, A. Grinthal, N. He, D. Fox, J. C. Weaver and J. Aizenberg, *Nature*, 2016, **531**, 78–82.
18 P. Kim, T.-S. Wong., J. Alvarenga, M. J. Kreder, W. E. Adorno-Martinez and J. Aizenberg, *ACS Nano*, 2012, **6**, 6569–6577.
19 T. Kajiya, F. Schellenberger, P. Papadopoulos, D. Vollmer and H.-J. Butt, *Sci. Rep.*, 2016, **6**, 23687.
20 Y. S. Kim, K. Y. Suh and H. H. Lee, *Appl. Phys. Lett.*, 2001, **79**, 2285.
21 S. Wooh, H. Yoon, J.-H. Jung, Y.-G. Lee, J. H. Koh, B. Lee, Y. S. Kang and K. Char, *Adv. Mater.*, 2013, **25**, 3111–3116.
22 S. Wooh, J. H. Koh, S. Lee, H. Yoon and K. Char, *Adv. Funct. Mater.*, 2014, **24**, 5550–5556.

23 H. M. Princen and S. G. Mason, *J. Colloid Sci.*, 1965, **20**, 246–266.
24 C. M. Knobler and D. Beysens, *Europhys. Lett.*, 1988, **6**, 707–712.
25 A. Steyer, P. Guenoun and D. Beysens, *Phys. Rev. E: Stat., Nonlinear, Soft Matter Phys.*, 1993, **48**, 428–431.
26 W. A. Gifford and L. E. Scriven, *Chem. Eng. Sci.*, 1971, **26**, 287–297.
27 D. Dushkin, P. A. Kralchevsky, H. Yoshimura and K. Nagayama, *Phys. Rev. Lett.*, 1995, **75**, 3454–3457.
28 P. A. Kralchevsky and K. Nagayama, *Adv. Colloid Interface Sci.*, 2000, **85**, 145–192.